

# FAST STEERING MIRROR FOR LASER COMMUNICATION

H. Langenbach, EADS Astrium GmbH, *harald.langenbach@astrium.eads.net*  
M. Schmid, EADS Astrium GmbH, *manfred.schmid@astrium.eads.net*

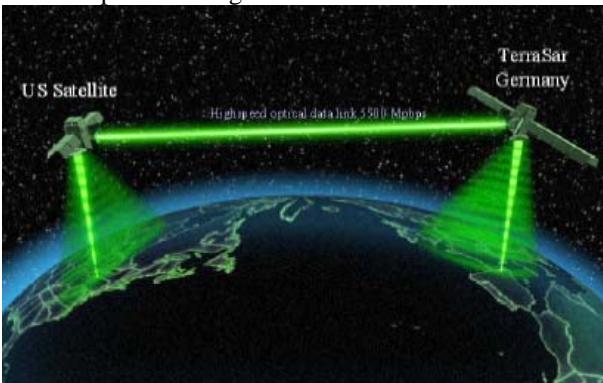
## Abstract

Future multimedia satellites require communication at large bandwidth which can be achieved by means of optical communication links. TESAT Spacecom is currently developing a Laser Communication Terminal (LCT) for such applications under DLR contract. EADS Astrium is developing and building the mechanisms for Pointing, Acquisition and Tracking (PAT) of the laser beam between two Laser Communication Terminals. Based on this development work the development of mechanism H/W to be flown on TerraSar X is currently under way.

After a short description of the general arrangement of the Mechanisms inside the LCT, the paper describes the design of the fast steering mirrors (FSM) reflecting the critical requirements and the solutions how to achieve them.

## 1. INTRODUCTION

The aim of the LCT-TSX project is to verify the terminals by an optical downlink from the TerraSar-X satellite to earth and in a second phase an inter-satellite link between TerraSar-X and an US Satellite. It is planned to achieve data rates up to 5.5 Gbps @ 8000 km. Optical links require a stable pointing of the laser beam even with disturbances coming from the satellite and an excellent wavefront quality (WFE) of the mirrors over a wide temperature range.



## 2. FUNCTIONAL ARRANGEMENT OF THE PAT MECHANISMS

The pointing function for the laser beam is divided in three different mechanisms. A coarse pointing assembly (CPA) provides the hemispherical coverage of the LCT. A fine pointing assembly (FPA) is responsible for tracking the incoming laser beam on the receiver (RXA) and for acquisition. The outgoing laser beam coming from the transmitter (TXA) passes a third mechanism, called Point Ahead Assembly (PAA). With this mirror a point ahead angle between received and transmitted laser beam can be adjusted. The point ahead angle is necessary due to the fact that the running time of the light cannot be neglected. FPA and PAA are fast steering mirrors.

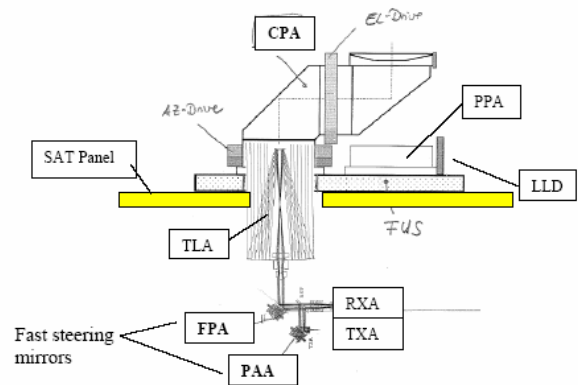


Fig.: 2-1: Functional Arrangement of the PAT Mechanisms

### 3. REQUIREMENTS FOR THE FAST STEERING MIRRORS

The main requirements divided in FPA and PAA requirements are listed in following subchapters. The most challenging requirements are dynamic performance, accuracy and waferfront error (WFE).

The dynamic performance determined by a high closed loop bandwidth has already been achieved in a technology pre-phase.

Optimisations were necessary in order to achieve the pointing accuracy and a perfect waferfront.

#### 3.1. Fast Steering Mirror (FPA) Requirements

Mass:	< 300 gr
Temperature Range:	-35°C to + 55°C
Design Load:	120 g
Radiation:	20 krad (SI)
Total Range (TR):	+/- 2.1 deg
Central Range(CR):	+/- 250 $\mu$ rad
Abs. Accuracy in TR	17.5 $\mu$ rad
Accuracy in FR	175 $\mu$ rad
Closed Loop Bandwidth:	$\geq$ 1000 Hz
WFE	15 nm RMS

#### 3.2. Point Ahead Assembly (PAA) Requirements

Mass:	< 300 gr
Temperature Range:	-35°C to + 55°C
Design Load:	120 g
Radiation:	20 krad (SI)
Total Range (TR):	7 mrad
Central Range(CR):	1 mrad
Abs. Accuracy in TR	50 $\mu$ rad
Abs. Accuracy in CR	17.5 $\mu$ rad
Rel. Accuracy in CR	5 $\mu$ rad
Closed Loop Bandwidth:	$\geq$ 1000 Hz
WFE	15 nm RMS

## 4. DESIGN DESCRIPTION

### 4.1. Design Approach

The FPA and PAA is designed as a stiff and light weight construction used to guide an incoming Laser-Beam as well as an outgoing Laser Beam to the telescope and CPU. The beams are to be reflected by a high precision mirror.

The design of the FPA is driven by the following aspects:

- No friction producing elements - low resistive torque
- Mirror rotation axes exactly 10 mm below the optical surface
- Mirror turning point in centre of gravity (COR = GOG)
- Spherical "linear" motors (high efficiency, linearity due to constant gap)
- Kardanic Suspension via flexural pivot elements
- Design optimised for easy integration, adjustment, and exchange of electrical components
- High stiffness / low mass
- Minimisation of moving masses

### 4.2. Design Description

The mechanism consists of a Rotor (Mirror and Magnets) which is gimbaled by 4 single flex pivots and a Stator which is basically a plate with 4 Stator Brackets carrying the motor coils and a housing with mounting interfaces (see Figure 4-1).

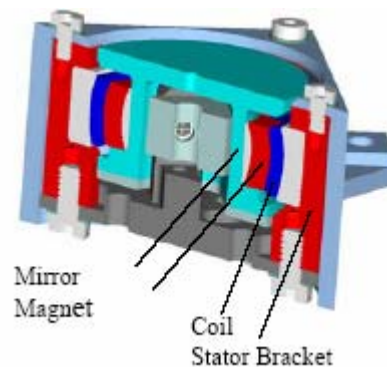


**Figure 4-1: Diagonal cut through the FPA**

In order to achieve maximum electrical efficiency and high linearity, special spherical customised motors have been developed. The FPA will be operated in closed loop, the position feed-back is given by 4 eddy current sensors.

Figure 4-2 shows a picture of the pre-integrated FPA w/o housing and related I/F flanges. In a subsequent and final integration step, the housing with the mechanical I/F will be mounted. The fully integrated FPA is shown in Figure 4-3.

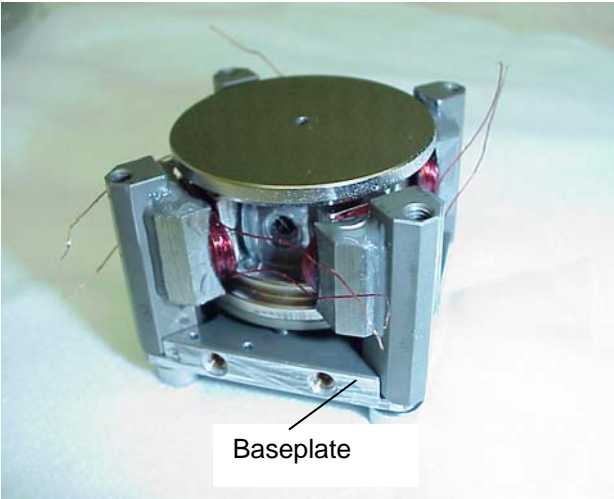


**Figure 4-2: Pre-integrated FSM (from technology phase)**

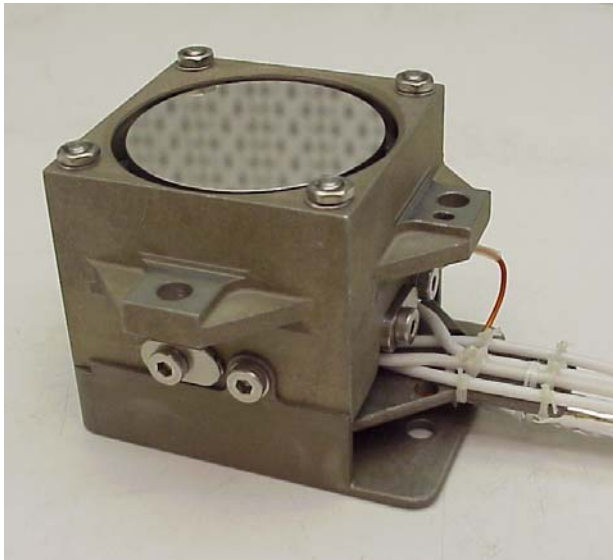


**Figure 4-3: Final integrated FSM (for ground station)**

#### 4.3. Description of Major FSM Components

##### 4.3.1. Baseplate/Housing

The driving factors for the structural parts of the FSM (the Housing and the Baseplate), were to achieve a high stiffness and low mass. This was realised by a design comprising only two integral parts taking over structural and I/F tasks. The Housing includes all mechanical outer interfaces and provides the structural support for the motor brackets.

The Baseplate provides the mounting I/F of the mirror axis and of the Motor Brackets. The Baseplate also includes the interfaces for the Sensors and the End Stops.

The selected material of all structural parts of the FSM is DISPAL S225 which has sufficient stiffness, high thermal conductivity and almost similar thermal expansion as the AlBeMet mirror.

##### 4.3.2. Drives

In order to achieve a high linearity over the required range of up to  $\pm 2.1$  deg and to optimise the electro-mechanical efficiency, special customised spherical motors have been developed. The drives have been verified by extensive development tests in the scope of the technology phase and found suitable without significant modifications for transfer to a flight model.

##### 4.3.3. Sensors

The built-in sensors of the FSM are eddy-current sensors by Kaman. These sensors have been selected because of high resolution and low noise within acceptable size. The sensor systems, 4 sensors per unit in differential target configuration and the drive electronics have been calibrated for the specific ranges and sensitivity of FPA and PAA. The differential target configuration makes the system tolerant against thermal distortions.

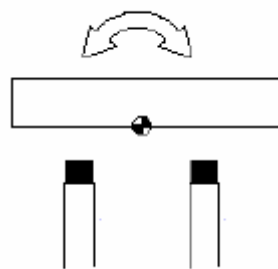


**Figure 4-4: Differential Target Configuration**

##### 4.3.4. Mirror with old design

The original material for the FSM mirror was AlBeMet. This material has been selected because of its high stiffness at low weight and good thermal conductivity. After

manufacturing of the blank, the blank has been coated with Ni, thermal cycled and polished. The surface finish is driven by the optical requirements and is realised as a thin silver coating additionally protected against corrosion. Figure 4-5 also shows the location of the pure aluminium targets for the eddy current sensors.

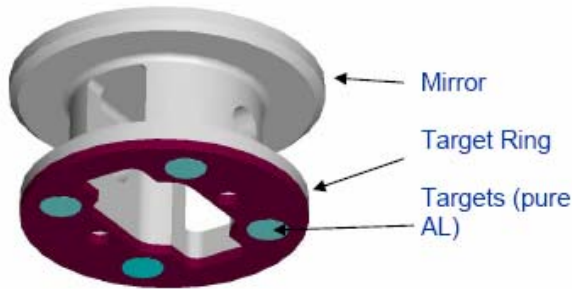


Figure 4-5: Old mirror design

## 5. OPTIMIZATIONS OF THE MIRROR BODY

### 5.1. Measurement and Analyses Results of the Mirror Body

First measurements and analyses of the mirror body have shown that the WFE requirements on  $\lambda/60$  cannot be achieved with the current mirror design. Although the design is a suitable solution for ground applications at a limited temperature range, the design needed to be improved for the use in a space environment with a large temperature range. Following different contributors to the WFE have been identified:

- CTE mismatch between magnets and AlBeMet mirror
- CTE mismatch between pivot, cardanic frame and mirror body
- CTE mismatch between mirror coating and mirror surface

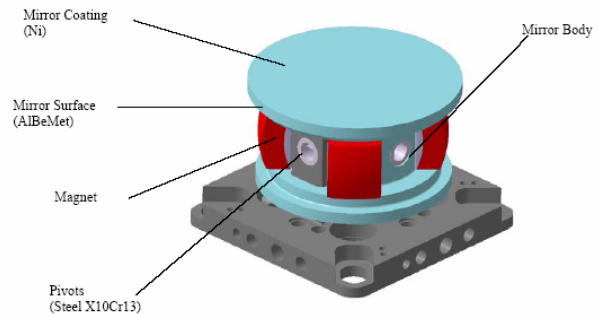


Figure 5-1: Contributors to WFE

### 5.2. Design Improvements to Flight Design

The easiest way to improve the design would have been to manufacture all parts of the same material, but in our case this was not possible. During a trade off we worked around with some isostatic mounts, but this approach was not promising in terms of envelope and dynamic behaviour. The final solution was a simple cut-in into the mirror body. The function of the cut in is to decouple the mirror surface from the deformations of the mirror body with the advantage that the re-design is limited to the mirror unit. Additional improvements in terms of stiffness were expected by changing the mirror material from AlBeMet to pure Beryllium.

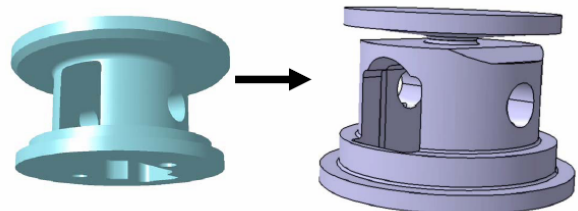
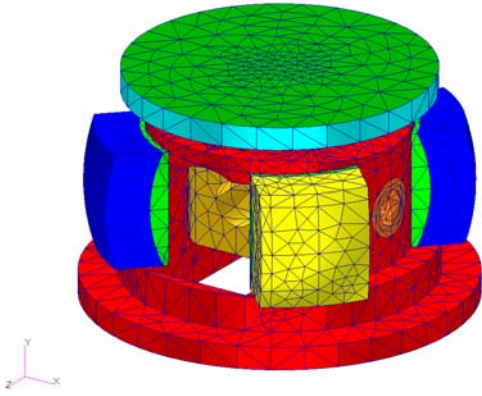


Figure 5-2: Design change to cut-in shape

### 5.3. Design Verification

The cut-in design has been analysed by FEM in terms of WFE and eigenfrequency under the specified thermal load-cases. Figure 5-3 shows the detailed FEM model for the FSM mirror containing all contributors to WFE and eigenfrequency of the mirror unit.



**Figure 5-3: FEM Model (groups colored)**

**5.3.1. WFE Prediction**

As expected, the result of the FEM analyses have shown a significant improvement of the WFE. After changing to the cut-in shape, the only remaining distributor for the WFE is the Ni layer thickness. The Ni layer thickness of the mirror coating has been specified to 50 μm on front, rear and the edges of the mirror.

load case	RMS error worst elliptic surface area (nm)
cool down to -35°C (Ni with 13.5E-6/K, 60μm on front, 50μm on rear and edge)	5,1
cool down to -35°C (Ni with 13.5E-6/K, 45μm on front, 35μm on rear and edge)	4,4
cool down to -35°C (without coating)	4,6
cool down to -35°C (Ni with 13.5E-6/K, 50μm on front, rear and edge)	2,4

**Table 5-1: Calculated WFEs for different contributors**

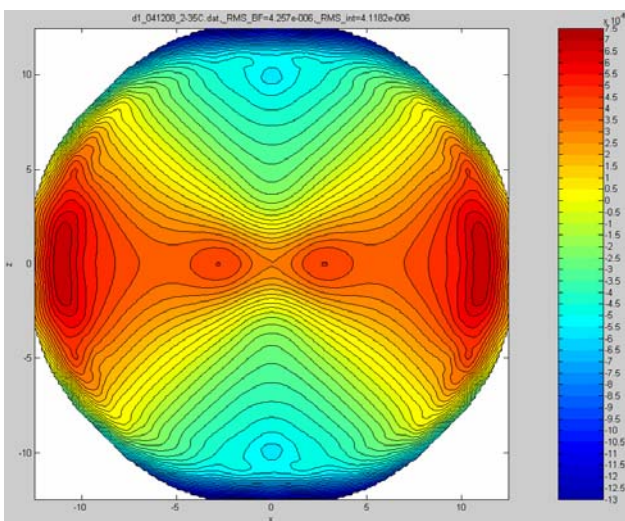


**Figure 5-4: Fringe plot of residual surface errors at -35°C 4.1 nm RMS**

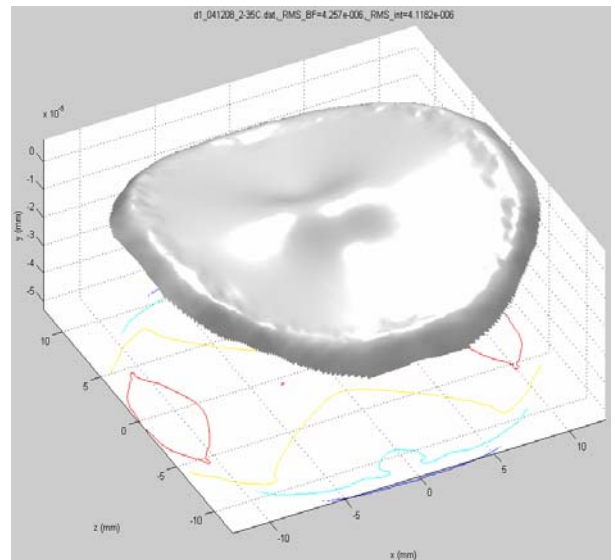


**Figure 5-5: Shape of residual surface errors at -35°C 4.1 nm RMS**

**5.3.2. Critical Eigenmode**

The critical eigenmode for the mirror is a tilt mode of the mirror surface which could lead to instability of the PAT controller when operating in the optical tracking loop. As a customer's requirement this eigenmode has to be above 20 kHz. Figure 5-6 shows that the current design also assures the specified stiffness leading to a eigenfrequency of 22 kHz.

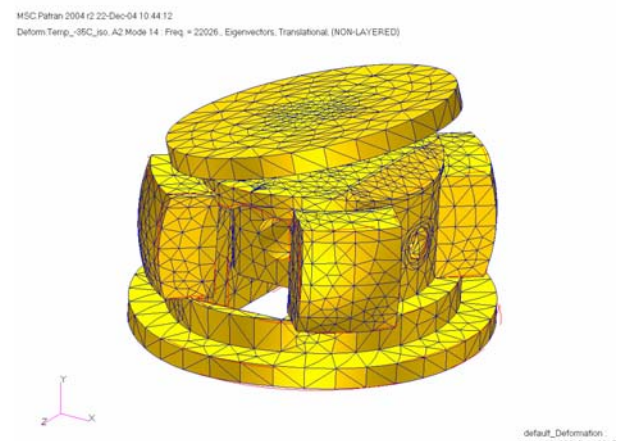


**Figure 5-6: Shape of the critical eigenmode at 22 kHz**

#### 5.4. Test Results of WFE Measurements

The WFE of the mirror as a function of temperature has been measured in the TV chamber at ASTRIUM. The preliminary test results have shown that the new design effectively reduces the WFE error as predicted. The measurement has also shown that settling effects of the material occurred leading to a remaining WFE error. Actually the manufacturing and coating process needs to be optimized by the manufacturer to eliminate this effect.

### 6. IMPROVEMENT OF POINTING ACCURACY

#### 6.1. FSM Calibration

During the technology phase it has been detected that different contributors make it very different to reach the specified pointing accuracy. The main contributors were

- Non-Linearity
- Cross-Talk
- Thermal drift of the sensors fixation
- Thermal drift of the sensor electronics

All the influences listed above except the thermal drift of the sensor fixation were repeatable errors, so they can be described mathematically and calibrated out. The thermal drift of the sensor fixation came from an un-optimized gluing process of the sensors into their bushings and forces applied by the sensor cable. ASTRIUM developed a mounting procedure that assures that the sensor fixation remains stable in the FSM. This could be achieved by modifications of the bushing design, the gluing process and the sensor cable fixation. For the other effects a series of calibration measurements at more than 1200 pointing vectors over the full range of the FSM at different temperatures has been performed allowing us to generate a calibration table. For data logging and FSM control we used a realtime xPC Target system together with Matlab/Simulink.

#### 6.2. Test Results

The final pointing performance measurements at different temperatures could verify that with the calibration method the required accuracy could be achieved. Figure 6-2 shows a typical test result for pointing accuracy measurement of a FPA.

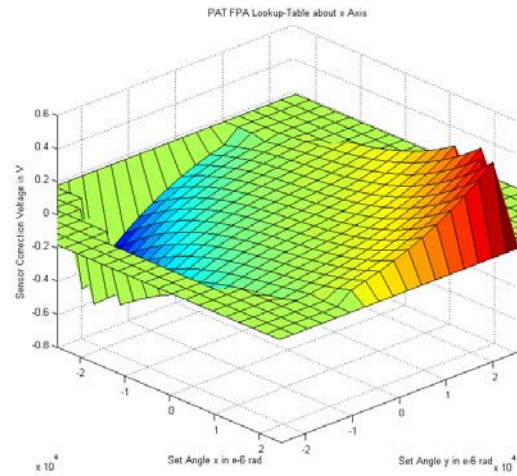


Figure 6-1: Example of FPA Calibration-Table

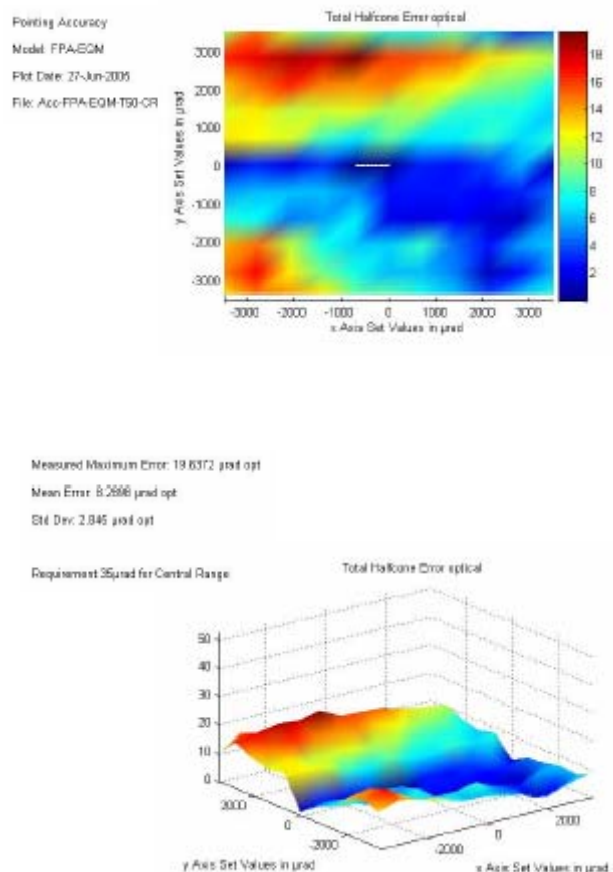


Figure 6-2: Typical Pointing Accuracy Plot (here at +55°C)

## **7. LESSONS LEARNED**

### **7.1. Wafer From Errors**

The cut-in method is an excellent possibility to decouple mirrors from external stresses. When the mirror is decoupled the major contributor to WFEs is the coating and the remaining stresses introduced during polishing. FEM analyses provide powerful tools to predict the WFE.

Stresses due to manufacturing, coating and polishing have the same order of influence like the CTE mismatch and need to be tracked, measured and eliminated by an appropriate manufacturing process and material selection.

### **7.2. Pointing Accuracy**

For high accuracy pointing tasks it is easier to characterize and calibrate a system, than to try to manufacture the "perfect" mechanism without non-linearity's and crosstalk. To be efficient with the characterization it is necessary to have state of the art measurement equipment and software. It has been pointed out that especially the xPC target system from Mathworks could be such a powerful tool.